Article

Systematic Incorporation of Gold Nanoparticles onto Mesoporous Titanium Oxide Particles for Green Catalysts

Jian Hou [1,†] **, Wongi Jang** [2,3,†] **, Jaehan Yun** [2,3] **, Franklin O. Egemole** [2] **, Dianguo Geng** [1] **, Hongsik Byun** [3,*] **, Dong-Woo Kang** [4,*] **and Jun-Hyun Kim** [2,*]

[1] Department of Chemical Engineering, Zibo Vocational Institute, Zibo 255314, China; houjimmy@naver.com (J.H.); gengdianguo@hotmail.com (D.G.)
[2] Department of Chemistry, Illinois State University, Normal, IL 61790, USA; 508compo@daum.net (W.J.); ruri7220@naver.com (J.Y.); foegem1@ilstu.edu (F.O.E.)
[3] Department of Chemical Engineering, Keimyung University, Daegu 42601, Korea
[4] Department of Electronic and Electrical Engineering, Keimyung University, Daegu 42601, Korea
* Correspondence: hsbyun@kmu.ac.kr (H.B.); dwkang@kmu.ac.kr (D.-W.K.); jkim5@ilstu.edu (J.-H.K.); Tel.: +1-309-438-2604 (J.-H.K.)
† Jian Hou and Wongi Jang have contributed equally to this work.

Abstract: This report describes the systematic incorporation of gold nanoparticles (AuNPs) onto mesoporous TiO_2 (MPT) particles without strong attractive forces to efficiently serve as reactive and recyclable catalysts in the homocoupling of arylboronic acid in green reaction conditions. Unlike using nonporous TiO_2 particles and conventional SiO_2 particles as supporting materials, the employment of MPT particles significantly improves the loading efficiency of AuNPs. The incorporated AuNPs are less than 10 nm in diameter, regardless of the amount of applied gold ions, and their surfaces, free from any modifiers, act as highly reactive catalytic sites to notably improve the yields in the homocoupling reaction. The overall physical properties of the AuNPs integrated onto the MPT particles are thoroughly examined as functions of the gold content, and their catalytic functions, including the rate of reaction, activation energy, and recyclability, are also evaluated. While the rate of reaction slightly increases with the improved loading efficiency of AuNPs, the apparent activation energies do not clearly show any correlation with the size or distribution of the AuNPs under our reaction conditions. Understanding the formation of these types of composite particles and their catalytic functions could lead to the development of highly practical, quasi-homogeneous catalysts in environmentally friendly reaction conditions.

Keywords: mesoporous TiO_2; gold nanoparticle; homocoupling reaction; recyclable catalyst; deposition precipitation

1. Introduction

Nontoxic metal-based materials have been extensively fabricated to develop reactive catalysts that can be operational in environmentally friendly conditions for various chemical transformation reactions [1–5]. One attractive candidate is a colloidal form of nanoscale metal particles that can be prepared in green solution media (e.g., water and EtOH) and still show catalytic reactivity and recyclability [2,6–8]. Among many metal nanoparticles, gold nanoparticles (AuNPs) have shown ideal characteristics due to their biocompatible nature and well-established preparation strategies for diverse structures [2,9–13]. In this sense, bare and surface-modified AuNPs have been tested as catalysts in numerous chemical reactions, including dye degradation, reduction, oxidation, and coupling reactions [1,5,8,9,12,14,15]. However, designing catalytically active AuNPs and maintaining their reactivity in solution-based chemical reactions are still challenging tasks due to the limited surface areas and insufficient long-term stability. Integrating gold atoms and AuNPs onto solid supports can improve their stability as heterogeneous catalysts but results in
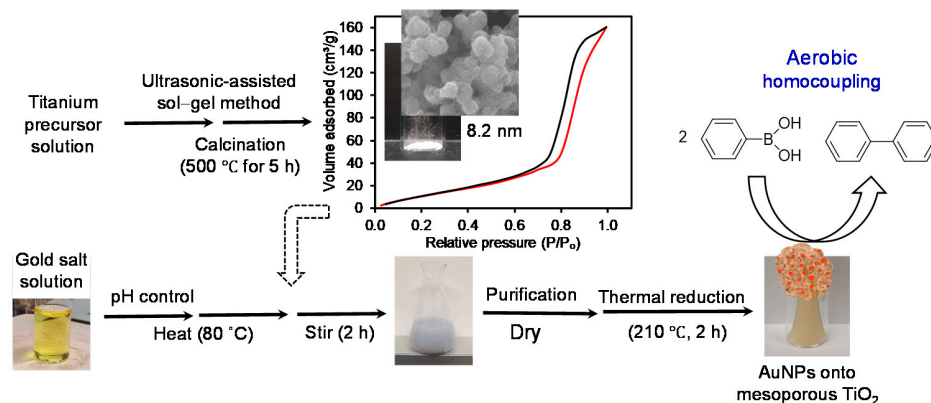
low reactivity and poor selectivity [1,3,16,17]. Comparably, gold-ligand-type clusters are being developed, showing high catalytic reactivity in several chemical reactions, however they still display problematic issues common of homogeneous catalysts associated with recycling and separation after reaction [1,3,17]. To minimize these common problems while harnessing the advantages of both catalysts, quasi-homogeneous (or quasi-heterogeneous) catalysts have been investigated to achieve the desired catalytic reactivity or selectivity (e.g., homogeneous catalyst) and recyclability or separability (heterogeneous catalyst) in green reaction conditions [3,10,11,18]. To fulfill the design of AuNP-based quasi-catalysts, readily available mesoporous TiO$_2$ (MPT) particles from many supporting materials have been selected to serve as host substances because of their large surface areas, long-term stability, good dispersity, and easy preparation in green solvents [3,4,9,19–21].

Here, we attempted to incorporate varying numbers of AuNPs onto MPT particles via deposition precipitation and examine their physicochemical properties, as well as their green catalytic functions. The physically loaded AuNPs exhibited improved stability in solution and possessed abundant bare surfaces that could ideally serve as catalytically active sites for diverse chemical reactions. Specifically, the systematic integration of AuNPs onto the MPT was accomplished simply by controlling the amount of applied gold salts. The degree of AuNP loading, the overall physical properties of the composite particles, and their catalytic properties were evaluated using the homocoupling of arylboronic acid in green conditions. As this type of C–C-bond-forming reaction requires a long reaction time, use of a base, and a relatively mild temperature, the prepared composite particles can be properly validated for their catalytic functions [12,22–24]. This homocoupling reaction is of particular interest due to the applicability to the production of fundamentally important chemicals, such as organic starting materials, drug molecules, bioactive heterocycles, and natural products [12,25–27]. Based on the C–C-bond-forming homocoupling reaction, the catalytic properties of various AuNP-loaded MPT particles were examined to understand their reactivity, recyclability, and activation energy (E$_a$) [11,16,25,27,28]. In addition, the recyclability of the composite particles and their applicability in the homocoupling of other arylboronic acids were tested in an environmentally friendly solvent (i.e., EtOH). It is important to remember that a simple wet chemical synthetic approach was utilized to prepare these composites in water, and their catalytic reactivity, selectivity, and recyclability were also established in EtOH under mild reaction conditions. As these composite particles have shown the advantages of both homogeneous and heterogeneous catalytic systems, these types of colloidal materials could eventually serve as practical quasi-catalysts under green reaction conditions. Thoroughly examining the structural features and catalytic activities of the composite particles helped provide a better understanding of their overall catalytic functions, which will allow for the development of high-yield, cost-effective, green catalytic systems.

2. Results and Discussion

Figure 1 shows the overall process of designing composite particles consisting of guest AuNPs and host MPT particles via a deposition precipitation method for their use as catalysts in the homocoupling of phenylboronic acid. Initially, the mesoporous characteristics of TiO$_2$ particles (i.e., pore size of 8.2 nm) were clearly supported by the presence of the hysteresis loop between the adsorption and desorption curves obtained using the BET isotherm test with N$_2$ gas. We also showed the possibility of integrating AuNPs onto mesoporous-type host particles for use as reactive catalysts. Here we have taken one further step by systematically controlling the amount of gold ions on the MPT particles (prepared using the ultrasonic-assisted sol–gel method) at 80 °C for 2 h [29,30]. After uptaking various concentrations of gold ions onto the MPT particles, free gold ions were removed using a simple purification step and the composite mixtures were completely dried. The series of the mixtures then underwent a temperature-induced reduction process at 210 °C in an oven to convert gold ions to AuNPs on the MPT particles. As this process does not require the use of any reducing or stabilizing agent that can easily bind to the
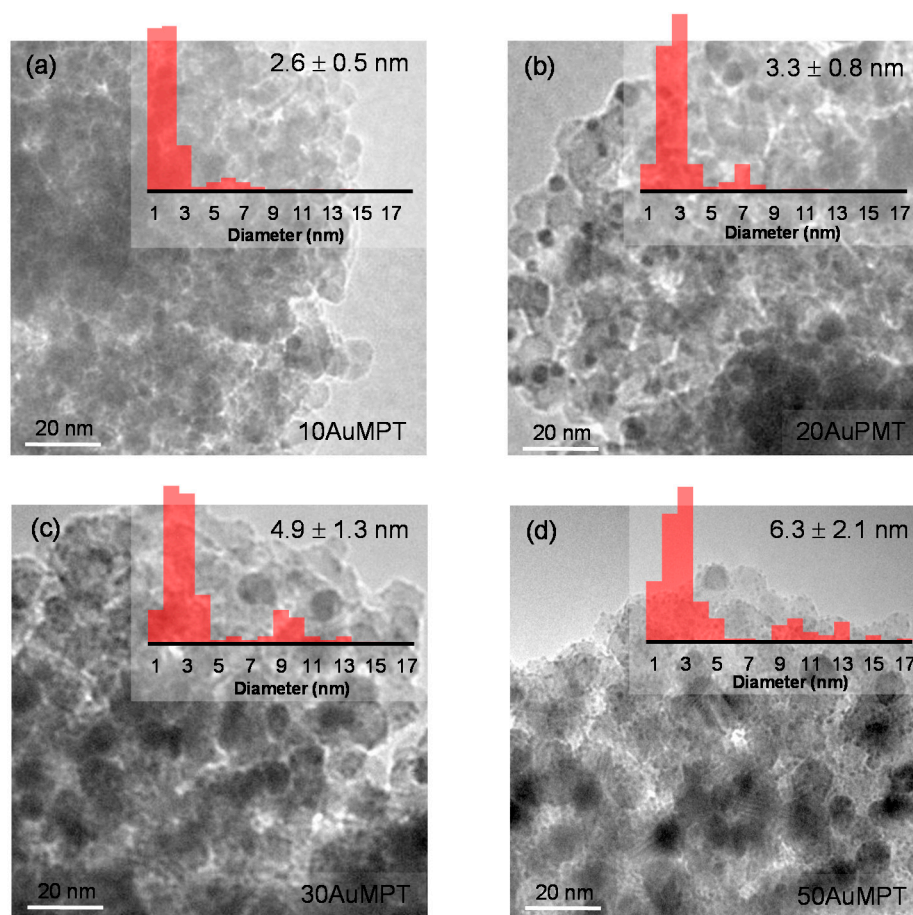
surfaces of AuNPs (e.g., could block catalytically active sites), these physically integrated AuNPs in the absence of surface modifiers should possess readily available surfaces on the host MPT particles. As the host MPT particles could improve the stability of the embedded AuNPs in solution, we speculated that these composite particles possessing small AuNPs with abundant free surfaces could serve as reactive catalysts in various chemical reactions.

Figure 1. The preparation of mesoporous TiO_2 (MPT) particles (SEM image and BET graph) and physically incorporated AuNPs on MPT particles via deposition precipitation.

Initially, the formation of various AuNPs on the MPT particles was completed by controlling the amounts of gold salts from 10 wt% to 50 wt% with respect to the MPT particles. Although the applied amounts of the gold ions were not necessarily loaded onto the MPT particles, the sample notations we used were based on the initial amount of gold salts (e.g., 10AuMPT for 10 wt% gold salts to MPT). The TEM images (Figure 2) show the general distribution of composite particles, whereby the incorporated AuNPs are randomly distributed throughout the MPT particles. The size and distribution of the AuNPs gradually increased as functions of the applied amount of gold salts. This gradually increased number of AuNPs was supported by the appearance of a greater number of darker spots (from Figure 2a–d), because Au atoms have a higher electron density than Ti atoms [31,32]. For all AuMPT composite particles, we speculated that the smaller AuNPs were mostly formed within the pores, while the larger AuNPs were randomly formed on the outsides of the pores (i.e., the average of these bimodal size distributions resulted in slightly higher standard deviations). As a control experiment, nonporous TiO_2 particles were equally treated with 20 wt% gold salts (i.e., 20AuT), where the loaded AuNPs examined by TEM analysis had a more unimodal distribution with a larger average size because AuNPs were possibly formed around the surfaces (Supplementary Figure S1).

To quantitatively analyze the loaded amounts of AuNPs, atomic absorption spectrophotometry (AAS) analysis was carried out after dissolving the AuNPs from the composite particles in a strong acid solution (i.e., a 1:1 ratio of HCl and HNO_3). Using the calibration curve obtained from a series of gold standard solutions (Supplementary Figure S2), the amounts of integrated Au atoms onto the MPT particles as a function of the applied gold salts ranging from 10 wt% to 50 wt% were calculated and are summarized in Table 1. Gradually increasing the amount of used gold salts generally resulted in increased loading of AuNPs onto the MPT particles. However, the loading efficiency of AuNPs notably declined when the applied amount of gold salts was higher than 20 wt%. Similarly, nonporous TiO_2 particles treated with 20 wt% gold salts showed significantly lower amounts of atomic Au, indicating a lower loading efficiency of the AuNPs.

Figure 2. TEM images of various AuNP-loaded MPT (mesoporous TiO$_2$) particles prepared via deposition precipitation as a function of the applied amount of gold salts: (**a**) 10 wt%; (**b**) 20 wt%; (**c**) 30 wt%; (**d**) 50 wt%.

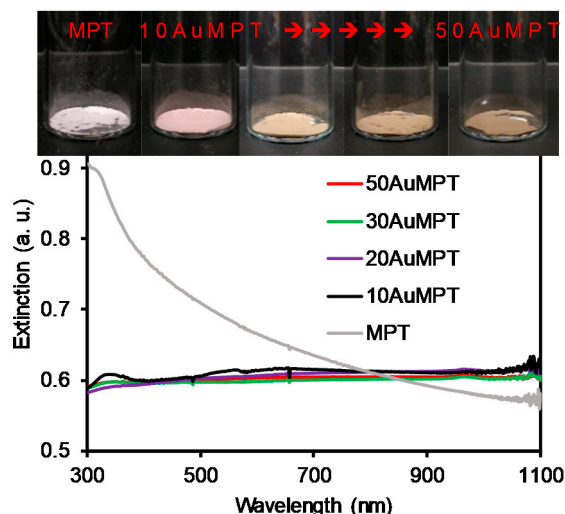**Table 1.** Preparation of composite particles as a function of the amount of gold salts.

	Gold Salts (wt%) with Respect to MPT				Nonporous TiO$_2$
	~10%	~20%	~30%	~50%	~20%
Mass of HAuCl$_4$ salts used	9.9 mg	19.7 mg	29.6 mg	49.3 mg	19.7 mg
Mass of atomic Au onto MPT	5.2 mg (53%)	11.6 mg (59%)	13.2 mg (45%)	15.9 mg (32%)	6.1 mg (31%)
Abbreviation	10AuMPT	20AuMPT	30AuMPT	50AuMPT	20AuT

Here, 8.05 mg (54%) of atomic Au was loaded when 14.8 mg of HAuCl$_4$ salts (~15%) was used; parentheses indicate loaded % of atomic Au with the respect to the applied gold salts.

Digital photos and absorption patterns of the MPT and composite particles were obtained as functions of the gold content (Figure 3). The color of the composite particles distinctively changed from light pink to brown; this observation could imply the gradual increase of the AuNP loading onto the MPT particles. Although many AuNPs containing nanoscale particles exhibit distinctive surface plasmon resonance (SPR) bands in the visible spectrum [8,9,33–35], these AuNPs incorporated on the MPT particles displayed flat SPRs across the entire wavelength. The near absence of detectable SPRs could be due to the relatively small size of the AuNPs formed within the pores and the scattering characteristics of the MPT host particles [36,37]. Similarly, the absorbance patterns relating to the MPT particles in the shorter wavelength range were notably reduced upon the

integration of AuNPs. However, the 20AuT composite particles showed a weak, broad SPR peak at 550 nm (characteristic of AuNPs) and a comparable absorption pattern at lower wavelengths (features of TiO_2 particles), implying the formation of relatively large AuNPs around the nonporous TiO_2 particles, which was confirmed by the TEM image (Supplementary Figure S1). The digital photo of the 20AuT composite particles shows the darkest color, implying the highest loading of AuNPs, however this observation could be due to the presence of AuNPs being mainly outside of the nonporous TiO_2 particles. This speculation was supported by the AA analysis shown above, demonstrating the inefficient loading of the AuNPs.
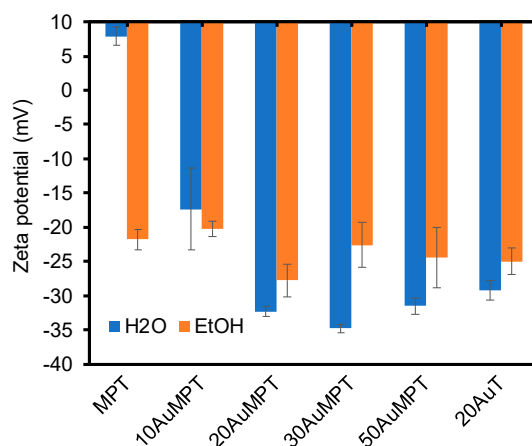

Figure 3. Digital photos and absorption patterns of bare MPT (mesoporous TiO_2) and various AuNP-loaded MPT composite particles.
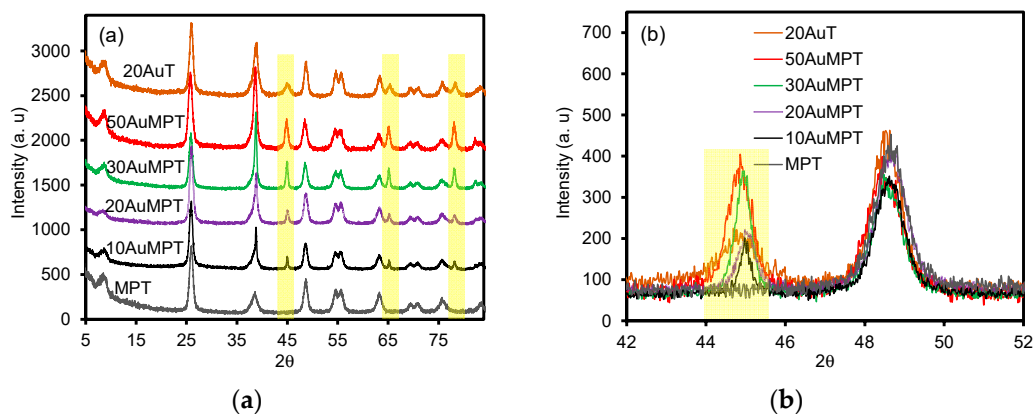
The surface charges of the MPT and composite particles were measured by a zeta potential analyzer (Figure 4). The charge of the MPT particles was almost neutral in pure water but became negative in EtOH (-24.2 ± 5.0 mV). Upon the integration of AuNPs onto the MPT particles, all composite particles, regardless of the solvents and AuNP content, displayed slightly negative potentials ranging from -15 mV to -35 mV, which were comparable to the literature values, suggesting moderate stability [38,39]. The FT-IR spectra were also collected for examination before and after the incorporation of AuNPs onto the MPT particles, whereby the identical vibrational patterns clearly (Supplementary Figure S3) implied the absence of any detectable stabilizers or capping agents (i.e., free from physico-chemical modification). It is important to remember that the absence of these randomly distributed and relatively small AuNPs across the MPT particles maximized the availability of their surfaces.

In addition, powder X-ray diffraction (PXRD) spectra were collected to examine how the AuNPs were incorporated onto the MPT particles as a function of the applied gold salts (Figure 5). The prominent XRD peaks of the MPT particles at $2\theta = 25.8°$, $38.5°$, $48.7°$, $54.9°$, $55.9°$, and $63.4°$ clearly presented the characteristic of anatase phase (Joint Committee on Powder Diffraction Standards (JCPDS) card 21-2172) [7,20,40,41]. Upon the loading of the AuNPs, the detectable peaks of AuNPs at $2\theta = 44.8$ and $65.2°$ for the (200) and (220) planes of the face-centered cubic gold with space group Fm3m were observed [10,42–44], while the crystallinity of the MPT particles remained the same. The strong characteristic peak of AuNPs at $2\theta = 38.3°$ for the (111) plane was not discernable due to the overlap with a broad TiO_2 peak and integration of relatively small AuNPs [20,40,44]. However, the peaks at $2\theta = 44.8$ and $65.2°$ evidently suggested the presence of AuNPs. The Scherrer equation ($d_{hkl} = \frac{k\lambda}{\beta \cos(\theta)}$, where $k = 0.89$ for the shape factor of spherical particles, $\lambda = 0.154$ nm of the X-ray, β = full width at half maximum of the peaks, and θ = the diffraction angle) was employed to estimate the size of the incorporated AuNPs [45,46]. Based on the rough

metric analysis, the steady increase of the peak widths as a function of the gold salt amount indicated the gradual increase of the integrated AuNPs in size (examples of AuNP size calculations are available on the last page of the Supplementary Materials section). This interesting observation somewhat contradicted the results obtained by the TEM images, which is currently under investigation. On the other hand, it is noticeable that the gradual increase in the peak intensity obviously indicated increased loading of AuNPs onto the MPT particles as a function of the gold salt amount. Similarly, the crystallite size of the MPT particles before and after the integration of AuNPs could also be calculated using the peaks at $2\theta = 25.8°$, $48.7°$, and $63.4°$, but no obvious changes of the peak widths strongly suggested the negligible influence on the size of the host MPT particles.

Figure 4. Zeta potentials of bare MPT (mesoporous TiO_2) and various AuNP-loaded MPT composite particles in water and EtOH. (Note: AuT, AuNPs onto nonporous TiO_2 particles).

(a)

(b)

Figure 5. PXRD patterns of bare MPT (mesoporous TiO_2 and various AuNP-loaded MPT composite particles: (**a**) offset scale spectra for clear presentation; (**b**) overlayed and expanded spectra to compare peak widths (highlights in yellow indicate peaks from AuNPs). (Note: AuT, AuNPs onto nonporous TiO_2 particles).

The thermogravimetric analyzer and differential scanning calorimetry (a dual TGA–DSC system) were utilized to examine the thermal stability of the composite particles (Supplementary Figure S4). All composite particles exhibited insignificant weight loss (by TGA) and heat flow (by DSC) patterns, as the initial TiO_2 particles were calcined to produce a mesoporous structure prior to AuNP loading. No clear weight loss associated with volatile organic species or any functional groups indicated that the composite particles solely consisted of the MPT particles and AuNPs. This observation also showed that our synthetic approach readily allowed for the physical integration of AuNPs onto the MPT particles, whereby the abundant free surfaces of the AuNPs without any capping agents could potentially serve as reactive catalysts in various chemical reactions.
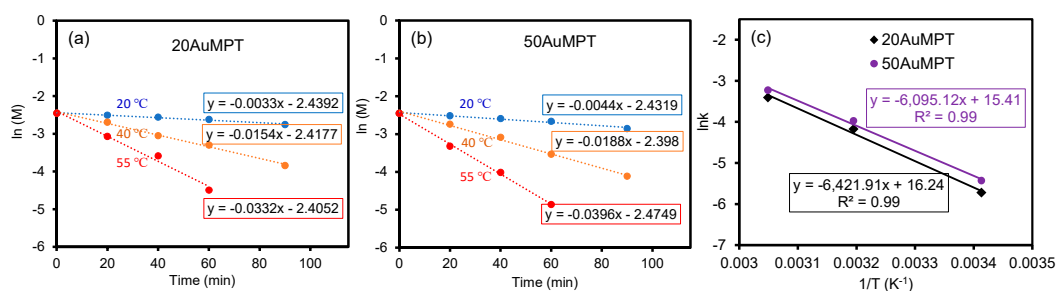
After the characterization of physicochemical properties, the composite particles were tested as catalysts in the homocoupling of phenylboronic acid. As a direct comparison, an equal mass of the composite particles (e.g., 10 mg) was mixed with the phenylboronic acid reactant and K_2CO_3 base in EtOH; the yields of the biphenyl product are summarized in Table 2. The composite particles (except the 10AuMPT particles) show that the conversion of the reactants reached nearly 100% after 4 h under a mild reaction temperature (i.e., 55 °C). The yield of the reaction with the 10AuMPT particles was noticeably lower than that with 20 wt%. The 15 wt% AuMPT particles were prepared as a control and tested in the same reaction, which readily improved the yield (82% in 2 h). This additional experiment clearly indicated that applying slightly increased amounts of gold salts (i.e., 20AuMPT) onto the MPT particles resulted in a high-yield reaction in a short period of time under a mild reaction temperature. The use of a green organic solvent (e.g., EtOH) contributed to the improvement of the mass transfer of organic molecules (i.e., phenylboronic acid and biphenyl) to induce effective interactions with the surfaces of the integrated AuNPs onto the MPT particles, which has been explained by the collision theory [10,13,47,48]. It is also important to remember that EtOH as a solvent did not show detectable formation of common phenol byproducts, unlike the same reaction in water [28]. As a control experiment, nonporous TiO_2 and mesoporous SiO_2 particles treated with 20 wt% gold salts were tested as catalysts under the same reaction but exhibited relatively low yields, possibly due to the poor loading and relatively large size of the loaded AuNPs. Although elucidating the exact catalytically active species in AuNP-based catalysts is still a challenging task, the efficient homocoupling reaction of arylboronic acid molecules could be catalyzed by primary Au^0 and minor $Au^{\delta+}$ around the AuNPs onto MPT particles, which was also explained by other similar systems [12,13,24,49]. Our ongoing work involves the use of additional oxide-based materials possessing mesoporous structures (e.g., SiO_2, CeO_2, and Al_2O_3) to examine the effects of supports in the catalytic reaction [12,19,50].

Table 2. Homocoupling reaction of phenylboronic acid using the composite particles.

Composite Particles	Yield of Biphenyl		
	2 h	**4 h**	**4 h (at rt)**
10AuMPT	57	83	81
20AuMPT	96	>98	>98
30AuMPT	98	>98	>98
50AuMPT	98	>98	>98
20AuT (nonporous)	65	84	82
20 wt% Au-SiO₂ (mesoporous)	24	45	42

To thoroughly evaluate the catalytic properties (e.g., reaction rate and activation energy) of the composite particles, the homocoupling reaction was carried out using the 20AuMPT and 50AuMPT particles at three different temperatures to monitor the yields as functions of time (Figure 6). These studies were carried out in pure EtOH, whereby byproducts were not formed under our aerobic reaction conditions. Slightly changing the reaction temperatures notably influenced the reaction rate constants from the slope, which indicated the first-order reaction. These kinetic patterns allowed for the calculation of activation energy (E_a) for the composite particles, which was derived from Arrhenius plots by the relationship between the logarithm of the rate constant (k) and the inverse temperature (1/T). The apparent E_a of the reaction was calculated to be ~53.4 kJ/mol for the 20AuMPT particles and ~50.7 kJ/mol for the 50AuMPT particles, which was comparable

to the reported value range (27–61 kJ/mol) [13,27,48]. Although this marginally lower E_a implied that the homocoupling of phenylboronic acid over 50AuMPT is slightly easier than that over 20AuMPT under our reaction conditions, this marginal difference does not clearly provide distinct relationships between the structural features of the incorporated AuNPs (e.g., size and distribution) and E_a. We speculated that the abundant bare surfaces of the integrated AuNPs without any capping agents acted as catalytically active sites to show the comparable E_a values under our reaction conditions. Similar observations using structurally diverse PtNPs and AuNPs were also reported by previous research groups [16,51,52].
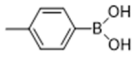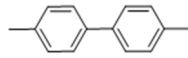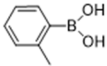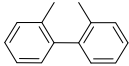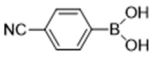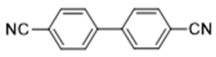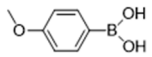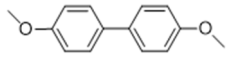

Figure 6. Reaction kinetics of (**a**) 20AuMPT (20 wt% AuNPs onto mesoprousTiO$_2$ particles) and (**b**) 50AuMPT (50 wt% AuNPs onto mesoprousTiO$_2$ particles), as well as (**c**) Arrhenius plots obtained from the absolute temperature (1/T) and the logarithm of reaction rates (lnk) to estimate the E_a values for the homocoupling of phenylboronic acid. All straight lines were drawn based on the best fit.

Considering the loading efficiency of AuNPs and their catalytic properties, the 20AuMPT particles were recycled at 55 °C in EtOH under aerobic conditions (Supplementary Figure S5). The use of EtOH readily allowed for the easy recovery of the composite particles after the reaction due to the good solubility of the organic reactant and product. Interestingly, these composite particles maintained a significant amount of activity at a minimum of six cycles while serving as a reactive quasi-homogeneous catalyst. The possible leaching of AuNPs from the MPT particles was evaluated by ICP-OES analysis after the 6th cycle (i.e., we collected the top solution of each cycle). Comparing the emission intensities of these collection solutions to the standard calibration curve (Supplementary Figure S6) showed the negligible loss of AuNPs (less than ~0.05 wt% loss for each batch). This insignificant loss of AuNPs did not impact their overall catalytic properties, although a slight change of the solution color was observed after 6 cycles.

Furthermore, additional homocouplings of arylboronic acids were tested under the same reaction conditions (Table 3), which resulted in reasonable yields without any byproduct formation (e.g., observed negligible levels of phenolic compounds). The homocoupling of 2-methylboronic acid showed the lowest yield due to the steric hindrance, while the slightly moderate conversions for 4-cynophenylboronic acid and 4-methoxyphenylboronic acid were possibly due to the limited solubility of the reactants and products in the EtOH conditions. As this homocoupling reaction for various arylboronic acids was not fully optimized, our ongoing effort involves the screening of different solvents, inorganic bases, and reaction temperatures. Our future studies will also cover the surface modification of composite particles with self-assembled monolayers to greatly improve their dispersity in various solvents (Supplementary Figure S7). More precise control of their physical properties in various solvents could provide the integrated AuNPs with new catalytic features. In addition, the use of MPT particles as host materials can have great advantages for the development of reactive quasi-homogeneous catalysts. Overall, the structural features of incorporated AuNPs can be further regulated to precisely control the physicochemical properties and to provide a better perspective in designing reactive, selective, and recyclable catalysts for various chemical reactions.

Table 3. Homocoupling reaction of various arylboronic acids using 20AuMPT particles.

Reactant	Product	GC Yield (%)
		~92 (77)
		~39
		~72 [a]
		~68 [b]

Note: [a] extraction with acetonitrile; [b] extraction with toluene; trace level of byproduct formation ($\leq 1\%$); reaction at 55 °C for 4 h under aerobic conditions.

3. Materials and Methods

3.1. Materials

Phenylboronic acid, potassium carbonate (K_2CO_3), biphenyl, phenol, ethanol, isopropanol, titanium tetraisopropoxide (TIP, 98%), acetic acid, and hydrogen tetrachloroaurate trihydrate ($HAuCl_4 \cdot 3H_2O$) were obtained from Fisher Scientific (Waltham, MA, USA). 2-Methylphenylboronic acid (95%, TCI America, Portland, OR, USA), 4-methylphenylboronic acid (98%, Oakwood Chemical, Estill, Columbia, SC, USA), 4-cyanophenylboronoic acid (98%, eMolecules), 4-methoxyphenylboronic acid (98%, Acros, Carlsbad, CA, USA), 2,2′-dimethylbiphenyl (97%, Aldrich, St. Louis, MO, USA), 4,4′-dimethylbiphenyl (99%, Alfa Aesar, Tewksbury, MA, USA), 4,4′-biphenyldicarbonitril (97%, Aldrich, St. Louis, MO, USA), and 4,4′-methoxybiphenyl (>97%, Aldrich, St. Louis, MO, USA) were purchased from the indicated companies. Pure water was obtained from a Nanopure water system (Barnstead/Thermolyne) with a resistance of 18 MΩ.

3.2. Preparation of Composite Particles for Catalytic Homocoupling Reactions

Mesoporous TiO$_2$ (MPT) particles were initially prepared using a modified sol–gel method using TIP, isopropanol, and acetic acid [53,54]. Specifically, TIP (6.0 mL, 0.02 mol) was mixed with isopropanol (40.0 mL, 0.52 mol) via 10 min sonication. Acetic acid (4.2 mL, 0.07 mol) was then introduced to this clear solution and the sonication continued for an additional 60 min. After stirring the mixture for an additional 24 h at room temperature, the resulting milky white solution was filtered to remove unreacted materials and washed several times with DI water; the nanoparticles were dried at 80 °C in an oven. The resulting TiO$_2$ particles were calcined at 500 °C (with a ramping temperature of 5 °C/min) for 5 h to decompose the organic materials, resulting in the formation of MPT particles.

The integration of AuNPs onto MPT was accomplished via a slight modification of the deposition precipitation approach [34,46]. An aliquot (5.0 mL) of HAuCl$_4$ salts (10 mM, 0.0394 g/10 mL water) was mixed with 1 M KOH (0.4 mL) in a glass vial (~10.5 pH). After stirring at room temperature for 5 min, the vial was heated to 80 °C using an oil bath. The MPT particles (0.09 g) were carefully introduced to the mixture and stirred for an additional 2 h. After the mixture was cooled to room temperature, the resulting solution was centrifuged at 6000 rpm for 30 min three times to remove the free gold ions. The final precipitates were dried at 50 °C overnight. The purified powders were then thermally treated in an oven at 210 °C for 2 h prior to use as catalysts. The different amounts of AuNPs loaded onto the MPT particles were achieved by simply controlling the initial ratio of the HAuCl$_4$ salt and MPT particles.

3.3. Homocoupling Reactions

Dried powder (10 mg of the composite particles) was thoroughly mixed with phenylboronic acid (21 mg, 0.17 mmol) and K_2CO_3 (67 mg, 0.48 mmol) in EtOH (2.0 mL). The

reaction then proceeded under stirring at various temperatures (e.g., 55 °C) as a function of time. An aliquot (0.5 mL) of the reaction mixture was pipetted into an Eppendorf tube and separated by centrifugation at 10,000 rpm for 5 min. A small amount of octane was used as an internal standard for all samples. For the recyclability test, the composite particles were recollected by using the centrifugation (6000 rpm for 20 min) and washing (EtOH) steps twice.

3.4. Characterization

The general distribution of composite particles was characterized by transmission electron microscope (TEM, Hitachi H8100, Tokyo, Japan). All samples for the TEM analysis were deposited on 300 mesh carbon-coated copper grids. Some of collected images were used for the estimation of the size of integrated AuNPs (excluded extreme outliners) using the free ImageJ program (v1.45 s). The optical extinction of composite particles was obtained by a UV-visible spectrometer (Agilent, Santa Clara, CA, USA) over the wavelength range of 200 to 1100 nm after dispersing them in water or EtOH. The surface charges of composite particles in EtOH (~0.05 mg/mL) were examined with a zeta potential instrument (ZetaPALS, Brookhaven Instruments Corp., Holtsville, NY, USA). All collected data were averaged from a minimum of five measurements. Fourier-transform infrared spectroscopy (Spectrum 100 FT-IR Spectrometer, PerkinElmer, Waltham, MA, USA) spectra of bare MPT and composite particles were obtained in the scan range of 4000 to 650 cm^{-1} using an attenuated total reflection (ATR) sampling device. The amounts of AuNPs integrated onto the MPT particles were examined using an atomic absorption spectrophotometer (AAS, AAnalyst 200, Perkin Elmer) equipped with an Ag–Au hollow cathode lamp. A small quantity of composite particles (10 mg) was initially treated with a strong acid solution (1.0 mL of a 1:1 volume ratio of HCl-to-HNO$_3$) to dissolve the integrated AuNPs. After dilution with water, the mixture was centrifuged at 5000 rpm for 20 min and the top solution was subjected to the AA analysis. The leaching amount of AuNPs from the MPT particles after catalytic reactions was analyzed by inductively coupled plasmon–atomic emission spectroscopy (ICP-AES, Optima 8300, PerkinElmer). The absorbance and emission results were compared to those of standard solutions via the Beer-Lambert law. The thermal stability of the composite particles was tested with a dual thermogravimetric analyzer and differential scanning calorimetry (TGA-DSC, SDT Q600, TA Instrument, New Castle, DE, USA). A small quantity (3 mg) of dried composite particles (dried in an oven at 50 °C overnight) was placed in an alumina pan for the measurements (pre-heated at 80 °C for 10 min, ramping temperature of 25 °C/min from 80 to 800 °C under 50 mL/min N$_2$ gas). A PXRD system with Cu Kα radiation (MiniFlex 600, Rigaku Corp., Tokyo, Japan) was used to examine the crystalline features of composite particles (scan range: 3–80 degree, 0.02 steps, 5 degree/min). The specific surface area of MPT particles (after degassing at 200 °C for 2 h) was determined by the adsorption–desorption isotherms (BET) of liquid N$_2$ at −196 °C (Horiba SA-9600, HORIBA Scientific, Kyoto, Japan). The total pore volume was determined by the amount adsorbed at a relative pressure (P/P$_0$) and the pore size distribution was estimated using the BJH method. Gas chromatograms (GC, Thermo Focus GC chromatograph equipped with an FID detector and a fused silica capillary column, Thermo Scientific) were collected to examine the homocoupling reaction yields of arylboronic acid. A temperature programming method (a flow rate of 10 psi, a ramping rate of 25 °C/min from 130 °C to 250 °C, and inlet and detector temperatures of 250 °C) was used to determine the reaction yields, which were compared to the calibration curve of the biphenyl derivatives.

4. Conclusions

The deposition precipitation approach readily allowed for the systematic formation of small AuNPs onto the MPT particles. Simply controlling the amount of gold salts gradually influenced the loading efficiency of the AuNPs. After thorough characterization, the resulting composite particles were tested as catalysts in the aerobic homocoupling of arylboronic

acid in green reaction conditions, which greatly improved the overall reaction yields due to the presence of catalytically active sites coming from the abundant bare surfaces of physically incorporated AuNPs, which effectively interacted with the reactants. These high-yield reactions were also caused by the increased solubility of organic molecules in EtOH (e.g., improved mass transfer capability). Furthermore, the composite particles generally showed excellent recyclability and relatively good yields for the coupling of other aryl-boronic acid compounds. From the reaction kinetic studies at three different temperatures, these composite particles did not show a clear correlation between the apparent E_a and the size of incorporated AuNPs in this catalytic reaction. This interesting size-independent E_a is still under investigation. Understanding the way AuNPs are integrated onto the mesoporous host particles and examining their physiochemical and catalytic properties can lead to the development of reactive and recyclable quasi-homogeneous catalysts.

Supplementary Materials: The following are available online at https://www.mdpi.com/article/10.3390/catal11040451/s1, Figure S1: The general distribution of AuNPs incorporated onto the nonporous TiO_2 particles (20AuT) and the corresponding absorption patterns and digital photos. Figure S2: Calibration curves for the Au atom obtained by atomic absorption spectroscopy (AAS). Figure S3: FT-IR spectra of bare MPT and various AuNP-loaded MPT composite particles. Figure S4: Thermal properties of bare MPT and various AuNP-loaded MPT composite particles examined by (a) thermogravimetric analysis (TGA) and (b) differential scanning calorimetry (DSC). Figure S5: Yields of biphenyl by recycling 20AuMPT composite particles in the catalytic homocoupling of phenylboronic acid in EtOH. Figure S6: Calibration curves for the Au atom obtained by (a) atomic absorption spectroscopy (AAS) and (b) inductively coupled plasma–atomic emission spectroscopy (ICP-AES). Figure S7: Surface-modified 20AuMPT with hexadecanethiol in water, EtOH, and toluene. Examples of AuNP size calculations using the XRD peaks via the Scherrer equation.

Author Contributions: Conceptualization, J.H., W.J., D.-W.K. and J.-H.K.; methodology, W.J. and J.Y.; validation, W.J., J.Y. and F.O.E.; formal analysis, W.J. and J.Y.; investigation, J.H., W.J., J.Y. and F.O.E.; resources, J.H., D.G., H.B. and J.-H.K.; writing—original draft preparation, J.H. and W.J.; writing—review and editing, D.-W.K., H.B. and J.-H.K.; visualization, W.J. and D.-W.K.; supervision, H.B. and J.-H.K.; project administration, J.-H.K.; funding acquisition, D.G., D.-W.K. and H.B. All authors have read and agreed to the published version of the manuscript.

Data Availability Statement: Not applicable.

Conflicts of Interest: The authors declare no conflict of interest.

References

1. Astruc, D.; Lu, F.; Aranzaes, J.R. Nanoparticles as recyclable catalysts: The frontier between homogeneous and heterogeneous catalysis. *Angew. Chem. Int. Ed.* **2005**, *44*, 7852–7872. [CrossRef]
2. Narayan, N.; Meiyazhagan, A.; Vajtai, R. Metal nanoparticles as green catalysts. *Materials* **2019**, *12*, 3602. [CrossRef]
3. Prati, L.; Villa, A. Gold colloids: From quasi-homogeneous to heterogeneous catalytic systems. *Acc. Chem. Res.* **2013**, *47*, 855–863. [CrossRef] [PubMed]
4. Sharifi, T.; Mohammadi, T.; Momeni, M.M.; Kusic, H.; Rokovic, M.K.; Bozic, A.L.; Ghayeb, Y. Influence of photo-deposited Pt and Pd onto chromium doped TiO_2 nanotubes in photo-electrochemical water splitting for hydrogen generation. *Catalysts* **2021**, *11*, 212. [CrossRef]
5. Hernández, R.; Hernández-Reséndiz, J.R.; Cruz-Ramírez, M.; Velázquez-Castillo, R.; Escobar-Alarcón, L.; Ortiz-Frade, L.; Esquivel, K. Au-TiO_2 synthesized by a microwave- and sonochemistry-assisted sol-gel method: Characterization and application as photocatalyst. *Catalysts* **2020**, *10*, 1052. [CrossRef]

6. Ferraz, C.P.; Braga, A.H.; Ghazzal, M.N.; Zieliński, M.; Pietrowski, M.; Itabaiana, J.I.; Dumeignil, F.; Rossi, L.M.; Wojcieszak, R. Efficient oxidative esterification of furfural using Au nanoparticles supported on group 2 alkaline earth metal oxides. *Catalysts* **2020**, *10*, 430. [CrossRef]

7. Solaiyammal, T.; Murugakoothan, P. Green synthesis of Au and the impact of Au on the efficiency of TiO$_2$ based dye sensitized solar cell. *Mater. Sci. Energy Technol.* **2019**, *2*, 171–180. [CrossRef]

8. Liu, L.; Li, H.; Tan, Y.; Chen, X.; Lin, R.; Yang, W.; Huang, C.; Wang, S.; Wang, X.; Liu, X.Y.; et al. Metal-support synergy of supported gold nanoclusters in selective oxidation of alcohols. *Catalysts* **2020**, *10*, 107. [CrossRef]

9. Corma, A.; Garcia, H. Supported gold nanoparticles as catalysts for organic reactions. *Chem. Soc. Rev.* **2008**, *37*, 2096–2126. [CrossRef]

10. Eyimegwu, P.N.; Lartey, J.A.; Kim, J.-H. Gold-nanoparticle-embedded poly(N-isopropylacrylamide) microparticles for selective quasi-homogeneous catalytic homocoupling reactions. *ACS Appl. Nano Mater.* **2019**, *2*, 6057–6066. [CrossRef]

11. Jang, W.; Byun, H.; Kim, J.-H. Encapsulated gold nanoparticles as a reactive quasi-homogeneous catalyst in base-free aerobic homocoupling reactions. *ChemCatChem* **2019**, *12*, 705–709. [CrossRef]

12. Li, G.; Jin, R. Catalysis by gold nanoparticles: Carbon-carbon coupling reactions. *Nanotechnol. Rev.* **2013**, *2*, 529–545. [CrossRef]

13. Liu, C.-H.; Lin, C.-Y.; Chen, J.-L.; Lai, N.-C.; Yang, C.-M.; Chen, J.-M.; Lu, K.-T. Metal oxide-containing SBA-15-supported gold catalysts for base-free aerobic homocoupling of phenylboronic acid in water. *J. Catal.* **2016**, *336*, 49–57. [CrossRef]

14. De Rogatis, L.; Cargnello, M.; Gombac, V.; Lorenzut, B.; Montini, T.; Fomasiero, P. Embedded phases: A way to active and stable catalysts. *ChemSusChem* **2010**, *3*, 24–42. [CrossRef]

15. Ongartkit, A.; Ananta, S.; Srisombat, L. Preparation of Ag/Au/Pt nanoparticles and their catalytic properties. *Chem. Phys. Lett.* **2014**, *605–606*, 85–88. [CrossRef]

16. Murzin, D.Y. On apparent activation energy of structure sensitive heterogeneous catalytic reactions. *Catal. Lett.* **2019**, *149*, 1455–1463. [CrossRef]

17. Panigrahi, S.; Basu, S.; Praharaj, S.; Pande, S.; Jana, S.; Pal, A.; Ghosh, S.K.; Pal, T. Synthesis and size-selective catalysis by supported gold nanoparticles: Study on heterogeneous and homogeneous catalytic process. *J. Phys. Chem. C* **2007**, *111*, 4596–4605. [CrossRef]

18. Abu-Reziq, R.; Alper, H. Magnetically separable base catalysts: Heterogeneous catalysis vs. quasi-homogeneous catalysis. *Appl. Sci.* **2012**, *2*, 260–276. [CrossRef]

19. Willis, N.G.; Guzman, J. Influence of the support during homocoupling of phenylboronic acid catalyzed by supported gold. *Appl. Catal. A* **2008**, *339*, 68–75. [CrossRef]

20. Machin, A.; Cotto, M.; Ducongé, J.; Arango, J.C.; Morant, C.; Márquez, F. Synthesis and characterization of Au@TiO$_2$ NWs and their catalytic activity by water splitting: A comparative study with Degussa P25. *Am. J. Appl. Sci.* **2017**, *10*, 298–311. [CrossRef]

21. Kadam, A.N.; Salunkhe, T.T.; Kim, H.; Lee, S.-W. Biogenic synthesis of mesoporous N–S–C tri-doped TiO$_2$ photocatalyst via ultrasonic-assisted derivatization of biotemplate from expired egg white protein. *Appl. Surf. Sci.* **2020**, *518*, 146194. [CrossRef]

22. Molnar, A. Efficient, selective, and recyclable palladium catalysts in carbon-carbon coupling reactions. *Chem. Rev.* **2011**, *111*, 2251–2320. [CrossRef]

23. Parmentier, T.E.; Dawson, S.R.; Malta, G.; Lu, L.; Davies, T.E.; Kondrat, S.A.; Freakley, S.J.; Kiely, C.J.; Hutchings, G.J. Homocoupling of phenylboronic acid using atomically dispersed gold on carbon catalysts: Catalyst evolution before reaction. *ChemCatChem* **2018**, *10*, 1853–1859. [CrossRef]

24. Tsunoyama, H.; Sakurai, H.; Ichikuni, N.; Negishi, Y.; Tsukuda, T. Colloidal gold nanoparticles as catalyst for carbon–carbon bond formation: Application to aerobic homocoupling of phenylboronic acid in water. *Langmuir* **2004**, *20*, 11293–11296. [CrossRef] [PubMed]

25. Carrettin, S.; Guzman, J.; Corma, A. Supported gold catalyzes the homocoupling of phenylboronic acid with high conversion and selectivity. Angew. *Chem. Int. Ed.* **2005**, *44*, 2242–2245. [CrossRef] [PubMed]

26. Dhital, R.N.; Murugadoss, A.; Sakurai, H. Dual roles of polyhydroxy matrices in the homocoupling of arylboronic acids catalyzed by gold nanoclusters under acidic conditions. *Chem. Asian J.* **2012**, *7*, 55–59. [CrossRef]

27. Wang, L.; Wang, H.; Zhang, W.; Zhang, J.; Lewis, J.P.; Meng, X.; Xiao, F.-S. Aerobic homocoupling of phenylboronic acid on Mg–Al mixed-oxides-supported Au nanoparticles. *J. Catal.* **2013**, *298*, 186–197. [CrossRef]

28. Wang, L.; Zhang, W.; Su, D.S.; Meng, X.; Xiao, F.-S. Supported Au nanoparticles as efficient catalysts for aerobic homocoupling of phenylboronic acid. *Chem. Commun.* **2012**, *48*, 5476–5478. [CrossRef]

29. Neppolian, B.; Wang, Q.; Jung, H.; Choi, H. Ultrasonic-assisted sol-gel method of preparation of TiO$_2$ nano-particles: Characterization, properties and 4-chlorophenol removal application. *Ultrason. Sonochem.* **2008**, *15*, 649–658. [CrossRef]

30. Swapna, M.V.; Haridas, K.R. An easier method of preparation of mesoporous anatase TiO$_2$ nanoparticles via ultrasonic irradiation. *J. Exp. Nanosci.* **2016**, *11*, 540–549. [CrossRef]

31. Meijerink, M.J.; de Jong, K.P.; Zecevic, J. Growth of supported gold nanoparticles in aqueous phase studied by in situ transmission electron microscopy. *J. Phys. Chem. C* **2020**, *124*, 2202–2212. [CrossRef]

32. Akita, T.; Kohyama, M.; Haruta, M. Electron microscopy study of gold nanoparticles deposited on transition metal oxides. *Acc. Chem. Res.* **2013**, *46*, 1773–1782. [CrossRef]

33. Haiss, W.; Thanh, N.T.K.; Aveyard, J.; Fernig, D.G. Determination of size and concentration of gold nanoparticles from UV-vis spectra. *Anal. Chem.* **2007**, *79*, 4215–4221. [CrossRef]

34. Ma, Z.; Yin, H.; Overbury, S.H.; Dai, S. Metal phosphates as a new class of supports for gold nanocatalysts. *Catal. Lett.* **2008**, *126*, 20–30. [CrossRef]

35. Xiao, J.; Qi, L. Surfactant-assisted, shape-controlled synthesis of gold nanocrystals. *Nanoscale* **2011**, *3*, 1383–1396. [CrossRef] [PubMed]

36. Zhou, M.; Zeng, C.; Chen, Y.; Zhao, S.; Sfeir, M.Y.; Zhu, M.; Jin, R. Evolution from the plasmon to exciton state in ligand-protected atomically precise gold nanoparticles. *Nat. Commun.* **2016**, *7*, 13240. [CrossRef] [PubMed]

37. Chen, H.; Liu, C.; Wang, M.; Zhang, C.; Luo, N.; Wang, Y.; Abroshan, H.; Li, G.; Wang, F. Visible light gold nanocluster photocatalyst: Selective aerobic oxidation of amines to imines. *ACS Catal.* **2017**, *7*, 3632–3638. [CrossRef]

38. Martins, P.; Kappert, S.; Le, H.N.; Sebastian, V.; Kuhn, K.; Alves, M.; Pereira, L.; Cuniberti, G.; Melle-Franco, M.; Lanceros-Mendez, S. Enhanced photocatalytic activity of Au/TiO$_2$ nanoparticles against ciprofloxacin. *Catalysts* **2020**, *10*, 234. [CrossRef]

39. Lin, X.; Li, J.; Ma, S.; Liu, G.; Yang, K.; Tong, M.; Lin, D. Toxicity of TiO$_2$ nanoparticles to Escherichia coli: Effects of particle size, crystal phase and water chemistry. *PLoS ONE* **2014**, *9*, e110247. [CrossRef] [PubMed]

40. Nafria, R.; de la Piscina, P.R.; Homs, N.; Morante, J.R.; Cabot, A.; Diaze, U.; Corma, A. Embedding catalytic nanoparticles inside mesoporous structures with controlled porosity: Au@TiO$_2$. *J. Mater. Chem. A* **2013**, *1*, 14170–14176. [CrossRef]

41. Vallejo, W.; Rueda, A.; Dıʼaz-Uribe, C.; Grande, C.; Quintana, P. Photocatalytic activity of graphene oxide—TiO$_2$ thin films sensitized by natural dyes extracted from Bactris guineensis. *R. Soc. Open Sci.* **2019**, *6*, 181824. [CrossRef]

42. Zhang, J.-G.; Zhang, X.-Y.; Yu, H.; Luo, Y.-L.; Xu, F.; Chen, Y.-S. Preparation, self-assembly and performance modulation of gold nanoparticles decorated ferrocene-containing hybrid block copolymer multifunctional materials. *J. Ind. Eng. Chem.* **2018**, *65*, 224–235. [CrossRef]

43. Rodríguez-Martínez, C.; García-Domínguez, A.E.; Guerrero-Robles, F.; Saavedra-Díaz, R.O.; Torres-Torres, G.; Felipe, C.; Ojeda-López, R.; Silahua-Pavón, A.; Cervantes-Uribe, A. Synthesis of supported metal nanoparticles (Au/TiO$_2$) by the suspension impregnation method. *J. Compos. Sci.* **2020**, *4*, 89. [CrossRef]

44. Yan, W.F.; Petkov, V.; Mahurin, S.M.; Overbury, S.H.; Dai, S. Powder XRD analysis and catalysis characterization of ultra-small gold nanoparticles deposited on titaniamodified SBA-15. *Catal. Commun.* **2005**, *6*, 404–408. [CrossRef]

45. Nepak, D.; Srinivas, D. Effect of alkali and alkaline earth metal ions on benzyl alcohol oxidation activity of titanate nanotube-supported Au catalysts. *RSC Adv.* **2015**, *5*, 47740. [CrossRef]

46. Zanella, R.; Delannoy, L.; Louis, C. Mechanism of deposition of gold precursors onto TiO$_2$ during the preparation by cation adsorption and deposition–precipitation with NaOH and urea. *Appl. Catal. A* **2005**, *291*, 62–72. [CrossRef]

47. Eyimegwu, P.N.; Kim, J.-H. Atypical catalytic function of embedded gold nanoparticles by controlling structural features of polymer particle in alcohol-rich solvents. *Nanotechnology* **2019**, *30*, 285704. [CrossRef] [PubMed]

48. Karanjit, S.; Ehara, M.; Sakurai, H. Mechanism of the aerobic homocoupling of phenylboronic acid on Au20-: A DFT study. *Chem. Asian J.* **2015**, *10*, 2397–2403. [CrossRef]

49. Straktakis, M.; Garcia, H. Catalysis by supported gold nanoparticles: Beyond aerobic oxidative processes. *Chem. Rev.* **2012**, *112*, 4469–4506. [CrossRef]

50. Fujitani, T.; Nakamura, I.; Akita, T.; Okumura, M.; Haruta, M. Hydrogen dissociation by gold clusters. *Angew. Chem. Int. Ed.* **2009**, *48*, 9515–9518. [CrossRef] [PubMed]

51. Fenger, R.; Fertitta, E.; Kirmse, H.; Thunemann, A.F.; Rademann, K. Size dependent catalysis with CTAB-stabilized gold nanoparticles. *Phys. Chem. Chem. Phys.* **2012**, *14*, 9343–9349. [CrossRef] [PubMed]

52. Sharma, R.K.; Sharma, P.; Maitra, A. Size-dependent catalytic behavior of platinum nanoparticles on the hexacyanoferrate(III)/thiosulfate redox reaction. *J. Colloid Interface Sci.* **2003**, *265*, 134–140. [CrossRef]

53. Niu, B.; Wang, X.; Wu, K.; He, X.; Zhang, R. Mesoporous titanium dioxide: Synthesis and applications in photocatalysis, energy and biology. *Materials* **2018**, *11*, 1910. [CrossRef] [PubMed]

54. Yoo, K.S.; Lee, T.G.; Kim, J. Preparation and characterization of mesoporous TiO$_2$ particles by modified sol–gel method using ionic liquids. *Microporous Mesoporous Mater.* **2005**, *84*, 211–217. [CrossRef]